

HUBBLE SPACE TELESCOPE IMAGING OF THE CIRCUMNUCLEAR ENVIRONMENTS OF THE CfA SEYFERT GALAXIES: NUCLEAR SPIRALS AND FUELING¹

RICHARD W. POGGE AND PAUL MARTINI²

Department of Astronomy, Ohio State University, 140 West 18th Avenue, Columbus, OH 43210-1173;
 pogge@astronomy.ohio-state.edu, martini@ociw.edu
 Received 2001 October 22; accepted 2001 December 28

ABSTRACT

We present archival *Hubble Space Telescope* (*HST*) images of the nuclear regions of 43 of the 46 Seyfert galaxies found in the volume-limited, spectroscopically complete CfA Redshift Survey sample. Using an improved method of image contrast enhancement, we create detailed high-quality “structure maps” that allow us to study the distributions of dust, star clusters, and emission-line gas in the circumnuclear regions (100–1000 pc scales) and in the associated host galaxy. Essentially all of these Seyfert galaxies have circumnuclear dust structures with morphologies ranging from grand-design two-armed spirals to chaotic dusty disks. In most Seyfert galaxies there is a clear physical connection between the nuclear dust spirals on hundreds of parsec scales and large-scale bars and spiral arms in the host galaxies proper. These connections are particularly striking in the interacting and barred galaxies. Such structures are predicted by numerical simulations of gas flows in barred and interacting galaxies and may be related to the fueling of active galactic nuclei by matter inflow from the host galaxy disks. We see no significant differences in the circumnuclear dust morphologies of Seyfert 1s and 2s, and very few Seyfert 2 nuclei are obscured by large-scale dust structures in the host galaxies. If Seyfert 2s are obscured Seyfert 1s, then the obscuration must occur on smaller scales than those probed by *HST*.

Subject headings: galaxies: active — galaxies: nuclei — galaxies: Seyfert

1. INTRODUCTION

There is now a large and compelling body of observational evidence that suggests that most, if not all, galaxies contain supermassive black holes at their centers (e.g., Richstone et al. 1998). Active galactic nuclei (AGNs), however, are found only in a small minority of all galaxies in the local universe (e.g., Huchra & Burg 1992; Ho, Filippenko, & Sargent 1997). What is it that makes some galaxies AGNs but most others quiescent? One line of inquiry is to ask if the differences are to be found in their circumnuclear environments. In particular, is the difference simply a matter of whether or not the central black hole is being provided with interstellar gas to fuel the nuclear activity?

The problem of providing fuel to an AGN from the vast reservoirs of interstellar gas found in the disks of spiral galaxies is how to remove the angular momentum from the gas so it can fall into the nucleus. The two classical mechanisms that are invoked are interactions (Toomre & Toomre 1972) and bars (Schwartz 1981), including nuclear bars (Shlosman, Frank, & Begelman 1989; Pfenniger & Norman 1990). There is an extensive literature devoted to demonstrating that both are theoretically viable mechanisms for fueling AGNs (Hernquist 1989; Barnes & Hernquist 1991; Athanassoula 1992; Friedli & Benz 1993; Piner, Stone, & Teuben 1995; Hernquist & Mihos 1995). Neither interactions nor bars of either type, however, are sufficiently common among AGNs compared to non-AGN galaxies to

be the fueling mechanism in all cases (Adams 1977; Petrosian 1982; Keel et al. 1985; Fuentes-Williams & Stocke 1988; Kotilainen et al. 1992; McLeod & Rieke 1995; Keel 1996; Alonso-Herrero, Ward, & Kotilainen 1996; Mulchaey & Regan 1997; DeRobertis, Hayhoe, & Yee 1998; Regan & Mulchaey 1999; Knapen, Shlosman, & Peletier 2000; Schmitt 2001; Laine et al. 2002).

Previous investigations have used the *Hubble Space Telescope* (*HST*) to study the circumnuclear environments of Seyfert galaxies and search for differences between the Seyfert galaxies with and without broad-line components. Nelson et al. (1996) obtained pre-Corrective Optics Space Telescope Axial Replacement imaging of a large sample of Seyfert and non-Seyfert Markarian galaxies to look for differences in the nuclear structure of these galaxies at higher angular resolution than is possible with ground-based imaging. They discovered that the nuclei of broad-line Seyfert 1–1.5 galaxies are dominated by strong point sources. In contrast, Seyfert 2s and other Markarian galaxies that lack broad-line regions contained weak or no strong nuclear source superposed on the underlying galaxy’s surface brightness profile. This result is further borne out in the extensive *HST* snapshot program of Malkan, Gorjian, & Tam (1998). They also invariably find more strong central point sources in Seyfert 1s than in the Seyfert 2s. Since this survey was carried out with the unaberrated Wide Field Planetary Camera 2 (WFPC2), these investigators were also able to look for differences in the nuclear environments of these galaxies. They found that Seyfert 2s were more likely to possess dusty nuclear environments than Seyfert 1s, lending support to unified models that propose obscuration of the broad-line region in Seyfert 2s by dust. Their observations are evidence for the presence of dust on large scales in the nuclear region, not in a torus immediately outside the broad-line region.

¹ Based on observations made with the NASA/ESA *Hubble Space Telescope*, obtained from the data archive at the Space Telescope Science Institute. STScI is operated by the Association of Universities for Research in Astronomy, Inc., under the NASA contract NAS 5-26555.

² Current address: Carnegie Observatories, 813 Santa Barbara Street, Pasadena, CA 91101.

Visible near-infrared color maps obtained with *HST* have shown that the circumnuclear (~ 100 – 1000 pc) regions of a large number of low-luminosity AGNs contain nuclear spiral dust lanes. These spirals are distinct from the spiral arms on kiloparsec scales in the main galaxy disk. V – H color maps of these galaxies show that these “nuclear spirals” extend from hundreds of parsec scales into the unresolved nucleus (Quillen et al. 1999; Regan & Mulchaey 1999). Theoretical models for the formation of nuclear spiral structure suggest that it is dynamically distinct from the main disk spiral arms (Bertin et al. 1989; Elmegreen, Elmegreen, & Montenegro 1992). Martini & Pogge (1999) showed that nuclear spirals in AGNs reside in non-self-gravitating disks and are therefore likely due to shocks in nuclear gaseous disks. They postulated that as shocks can dissipate energy and angular momentum, these nuclear spirals may be the signature of the fueling mechanism in these galaxies.

Nuclear spirals in AGNs have generally been seen mostly in Seyfert 2s, although this could easily be a selection effect; the samples of Quillen et al. (1999) and Regan & Mulchaey (1999) were mostly composed of Seyfert 2s. Also, Martini & Pogge (1999) only observed Seyfert 2s with NICMOS, since they have fainter nuclear point-spread functions (PSFs), and thus the circumnuclear environments of Seyfert 2s are easier to study with *HST* than the circumnuclear environments of Seyfert 1s. The question remains, however, whether Seyfert 1s and 2s contain nuclear spirals with the same relative frequency, that is, nearly 100%, as seen in Seyfert 2s. Since we have only near-infrared NICMOS imaging of the Seyfert 2s in the CfA sample, we need to use an alternate technique to look for nuclear spiral structure in these Seyfert galaxies. In § 3, we discuss our data processing, and we introduce a technique for creating “structure maps” in § 4 that are an excellent surrogate for color maps for detecting small-scale dust-extinction and emission-line features present in the visible-band images. We then use this technique to compare the circumnuclear environments of the Seyfert 1s and 2s in §§ 5 and 6, connecting the nuclear structures seen to the larger host galaxies in most cases. In § 7, we present a summary of our results and discuss the implications for the fueling of the active nuclei.

2. SAMPLE SELECTION

A limiting factor in statistical studies of Seyfert galaxies is the notorious difficulty of identifying a homogeneous sample free of crippling selection biases. Since Seyfert galaxies are identified primarily by their line spectra, one way to be absolutely certain of completeness is to take a spectrum of *every* galaxy down to some sensible magnitude limit. At present, the largest spectroscopically complete host-galaxy selected sample of Seyfert galaxies is the Huchra & Burg (1992) sample derived from the CfA Redshift Survey (Huchra et al. 1983). While not ideally homogeneous, its selection criteria are nonetheless very well understood. The CfA survey obtained optical spectra of a complete sample of 2399 galaxies down to a limiting photographic magnitude of $m_{Zw} \leq 14.5$ in fields limited to $\delta \geq 0^\circ$ and $b_{II} \geq 40^\circ$, and $\delta \geq -2.5^\circ$ and $b_{II} \leq -30^\circ$. This spectroscopically complete sample of Seyfert galaxies is reasonably large by AGN standards (46 galaxies) and relatively free of most of the usual selection biases, especially those against reddened AGNs that are inherent in traditional UV-excess surveys.

A further advantage of the CfA sample is that Osterbrock & Martel (1993) have obtained high signal-to-noise ratio (S/N) spectra of the nuclei of galaxies identified as having narrow lines (primarily Seyfert 2s). This provides us with a definitive set of spectral classifications for all of the CfA Seyfert galaxies with uniform depth. This important property is often overlooked in compiling samples of Seyfert galaxies. Much of the classification material in the literature is of mixed quality, especially for the intermediate types 1.5, 1.8, and 1.9 (Osterbrock 1981), where the broad-line component can be relatively weak. Without a carefully and homogeneously acquired set of classification spectra, a sample will be biased against the detection of nuclei with weak broad lines because such galaxies will be misclassified as Seyfert 2s. This is a potential problem with large samples selected out of the general catalogs without regard to the quality of the available classification material, especially if such samples are going to be used to examine the statistical properties of Seyfert galaxies with and without broad-line regions in direct spectra. A recent criticism of the CfA Seyfert sample is that it missed many low-luminosity AGNs with weaker emission lines due to the fact that the spectra were obtained for the purpose of redshift estimation (Ho & Ulvestad 2001). Our comparison of the circumnuclear regions of Seyfert 1s and 2s is thus based primarily on objects with relatively bright emission lines. In this paper we will refer to the Seyfert 1s and 1.5s collectively as the “Seyfert 1s” and the Seyfert 1.8s, 1.9s, and 2s collectively as the “Seyfert 2s.” This division reflects the fact that most of the 1.8s and 1.9s were at one time classified as Seyfert 2s and is thus a division between “strong broad lines” and “weak broad lines” rather than an arbitrary division among what is arguably a continuum of types. Lumping the 1.8s and 1.9s in with the “Seyfert 1s” would only have the effect of giving us a much smaller number of Seyfert 2s, but it does not otherwise affect our results significantly, as will become apparent.

The final virtue of this sample is that it is volume-limited. For all Seyfert types, V/V_m tests (Schmidt 1968) show that both Seyfert 1s and 2s have $\langle V/V_m \rangle \approx 0.5$ to within the uncertainties (Huchra & Burg 1992). Osterbrock & Martel (1993) repeated this analysis using different combinations of the various intermediate types, showing that this result is unaffected by how the Seyfert galaxies are subdivided into different types. The only systematic effect found thus far is that luminosity functions of the CfA Seyfert galaxies as a function of Seyfert type (Huchra & Burg 1992; Osterbrock & Martel 1993) show that the integrated (host+nucleus) luminosities of the Seyfert 1s are on average about 1 mag brighter than the Seyfert 2s. The results of Nelson et al. (1996) suggest that this is primarily the result of the systematically brighter Seyfert 1 nuclei.

Out of the 46 CfA Seyfert galaxies in our sample, 43 ($\sim 94\%$) have been imaged in broad bandpasses by *HST*/WFPC2. In general, the archival PC1 camera imaging in broadband filters (most of which are snapshots) constitutes a relatively uniform set of images with sufficient depth and spatial resolution to reveal detailed structures at subarcsecond scales in the nuclear regions. Most of these structures are expected to be caused by stars and dust in the host galaxy. Extended emission-line regions can also be seen in these broadband images if they are high surface brightness regions composed of essentially unresolved knots of emission, even though the bandpasses are broader than used in narrowband imaging work with *HST* (e.g., Pogge 1997).

These images will permit us to map out the immediate (a few hundred parsecs) environment of nearby Seyfert nuclei in a well-defined, spectroscopically complete sample of objects.

3. DATA COLLECTION AND PROCESSING

3.1. *WFPC2 Imaging Sample*

We have searched the *HST* archives for all publicly available WFPC2 images of the CfA Seyfert galaxies listed in Table 1 of Huchra & Burg (1992). We include Mrk 471, which was accidentally omitted from Huchra & Burg's Table 1 (but included in their analysis), and exclude the star-

burst galaxy Mrk 789 (Osterbrock & Martel 1993; Dahari & DeRobertis 1988). For this work, we have selected only those galaxies classified as Seyfert galaxies and neglected LINERs, X-ray galaxies, and QSOs. The Seyfert classifications are taken from the classifications given by Osterbrock & Martel (1993). The final sample of 46 galaxies, our adopted classifications, and the archival imaging parameters (exposure time, filter, and GO program ID) are listed in Table 1. Distances to each galaxy in Mpc are listed in column (7), computed by transforming the heliocentric radial velocities given by Huchra & Burg (1992) into the rest frame of the Local Group following Yahil, Tammann, & Sandage (1977) and adopting $H_0 = 75 \text{ km s}^{-1} \text{ Mpc}^{-1}$. Column (8) gives the projected scale in parsecs corresponding to $1''$ on

TABLE 1
CfA SEYFERT GALAXIES WITH ARCHIVAL WFPC2 IMAGING

Galaxy Name	Other	Seyfert Type ^a	Exposure (s)	Filter Name	<i>HST</i> Proposal ID	d_{75}^b (Mpc)	X_{75} (pc arcsec ⁻¹)	D_{25} (kpc)
Mrk 231		1	700	F814W	5982	165.3	801	63.4
Mrk 279		1	500	F606W	5479	124.1	602	31.4
Mrk 335	PG 0003 + 198	1	500	F606W	5479	106.8	518	9.8
Mrk 590	NGC 863	1	500	F606W	5479	106.8	518	33.3
Mrk 766	NGC 4253	1	500	F606W	5479	50.7	246	14.1
NGC 4051		1	500	F606W	5479	17.0	82	26.0
NGC 4235		1	500	F606W	5479	28.7	139	34.8
NGC 5940		1	500	F606W	5479	135.0	654	31.2
NGC 7469		1	500	F606W	5479	66.9	324	28.8
A0048 + 29	UGC 524	1	610	F814W	6361	147.0	713	38.1
Mrk 817		1.5	500	F606W	5479	127.6	620	24.0
Mrk 993		1.5	500	F606W	5479	65.1	316	41.4
NGC 3227		1.5	500	F606W	5479	20.6	100	32.2
NGC 3516		1.5	500	F606W	5479	38.9	189	19.7
NGC 4151		1.5	400	F547M	5433	20.3	98	37.3
NGC 5548		1.5	500	F606W	5479	67.0	325	28.2
NGC 6104		1.5	500	F606W	5479	113.5	550	27.5
NGC 7603	Mrk 530	1.5	500	F606W	5479	118.4	574	53.3
Mrk 334		1.8	500	F606W	5479	88.4	429	25.1
Mrk 471		1.8	500	F606W	5479	137.3	666	35.6
Mrk 744	NGC 3786	1.8	500	F606W	5479	36.1	175	23.0
UGC 12138	2237 + 07	1.8	500	F606W	5479	102.8	498	24.9
NGC 4395 ^c		1.9	600	F814W	6232	3.6	17	13.8
NGC 5033		1.9	460	F547M	5381	18.7	91	58.3
NGC 5252		1.9	500	F606W	5479	90.7	440	36.4
NGC 5273		1.9	460	F547M	5381	16.5	80	13.2
NGC 5674		1.9	500	F606W	5479	98.1	476	31.3
UM 146	0152 + 06	1.9	500	F606W	5479	71.6	347	26.2
Mrk 266SW	NGC 5256	2	500	F606W	5479	111.0	538	38.8
Mrk 270	NGC 5283	2	500	F606W	5479	38.2	185	11.9
Mrk 461	1335 + 34	2	560	F606W	8597	65.5	340	14.1
Mrk 573		2	500	F606W	5479	71.0	344	27.9
NGC 1068		2	500	F606W	5479	14.4	70	29.7
NGC 1144		2	500	F606W	5479	116.4	564	37.1
NGC 3362		2	500	F606W	5479	108.7	527	44.7
NGC 3982		2	500	F606W	5479	17.0	82	11.6
NGC 4388		2	560	F606W	8597	16.8	81	27.5
NGC 5347		2	500	F606W	5479	36.7	178	18.1
NGC 5695	Mrk 686	2	500	F606W	5479	56.9	276	25.6
NGC 5929		2	500	F606W	5479	38.5	187	10.7
NGC 7674	Mrk 533	2	500	F606W	5479	118.5	575	38.7
NGC 7682		2	500	F606W	5479	70.8	343	25.3
UGC 6100	A1058 + 45	2	500	F606W	5479	117.6	570	28.5

^a Osterbrock & Martel 1993.

^b See text; assumes $H_0 = 75 \text{ km s}^{-1} \text{ Mpc}^{-1}$.

^c Classification changed from 1.0 to 1.8 by Ho et al. 1997.

the sky at the distance of the galaxy. Archival *HST*/WFPC2 images of suitable quality for our purposes are available for 43 of the 46 CfA Seyfert galaxies. There is no archival WFPC2 imaging for three of the galaxies among the 46: Mrk 841, NGC 3080, and 1335+39. The absence of these galaxies from our sample does not significantly affect our results.

Most of the galaxies (35 out of 43) have 500 s F606W (wide *V*) band WFPC2 images obtained as part of a large *HST* Cycle 5 snapshot survey of AGNs (GO 5479, PI: Malkan). Images of the remaining galaxies are available from archival data of individual observations made by a variety of programs (Table 1, col. [6]). For these galaxies, we used the F547M or F814W filter (*I* band) images if F606W images were unavailable.

In the case of NGC 1068, all of the PC detector pixels in the central $2''$ – $3''$ of the nuclear region were completely saturated in the 500 s F606W snapshot image from GO 5479. For this reason, we also use the archival F547M images to recover information about the nucleus. These data consist of a pair of short integrations (140 and 300 s) that are not saturated. We will use these to probe structures closer than $\sim 1''$ and use the deeper F606W snapshot for the outer regions.

3.2. Post-Pipeline Image Processing

All of the WFPC2 images used in this study were already processed by the standard STScI reduction pipeline (described by Biretta et al. 1996). After inspection of the postpipeline images to verify that they were of acceptable quality for this study, the only additional processing steps required were removal of cosmic rays and treatment of saturation-related artifacts in the nuclei (destreaking). All of the galaxies selected had the active nucleus roughly centered in the PC detector, so we did not process any of the wide-field camera frames.

The majority of the images (35 of the 43) are snapshots acquired in a single exposure. In these cases, we used the COSMICRAYS task in the NOAO IRAF³ package to statistically remove most of the cosmic-ray events. Cosmic-ray events were defined as pixels deviating by more than 5σ above the local mean computed in a 7×7 pixel window and were replaced by the average of the 4 neighboring pixels. Any residual cosmic-ray events were hand cleaned from the final images with an interactive median-filtering tool in the XVISTA⁴ package.

For those galaxies with pairs of images of the same (or similar) integration time, we combined the images using a statistical differencing technique implemented as an XVISTA procedure script. This latter technique works as follows. The difference image formed by subtracting one image in the pair from the other consists primarily of positive and negative cosmic-ray hits, as the galaxy, foreground stars, and background all cancel to within the uncertainties. All pixels within $\pm 5\sigma$ of the mean residual background level

on the difference image are then set to zero (tagging them as unaffected by cosmic rays). A pair of cosmic-ray template images is then formed by separating the remaining positive and negative pixels. These templates are subtracted from the original images, and the two cosmic-ray-subtracted images are added together to form the final galaxy image.

A number of the images have the nuclei overexposed and saturated. We judged saturation by consulting the data quality file (DQF) that accompanies each WFPC2 image (Biretta et al. 1996). Two forms of saturation were encountered: pixels at or above the maximum A/D converter level (ADC saturation) and pixels that are so saturated they overflow the wells and bleed charge into adjacent pixels in their column (full-well saturation or “bleeding”). In our descriptions below, a nucleus was judged to be “completely saturated” if (1) it showed bleed streaks due to full-well saturation, or (2) the central 9 or more pixels were flagged as saturated in the DQF, corresponding to all pixels within the FWHM of the PC1 PSF in this band. In general, it takes only 1 or 2 pixels to be saturated in the core of the PSF to obviate deriving any useful quantitative photometry of the nucleus. For this reason, our analysis will concentrate on morphological characteristics. Bleed streaks of between 1 and 5 pixels in width appear in the most saturated nuclei and would complicate our structure-mapping analysis described in the following section if left alone. We destreaked these images via a simple method that successively interpolated across the streaks from the inside out until they were removed. No significant artifacts from the destreaking process are seen in our final structure maps.

4. STRUCTURE MAPS

Ideally, we would like to map the circumnuclear dust in these galaxies by creating photometric color maps from pairs of images taken at widely separated wavelengths, e.g., by making *V*–*H* color maps as we did in our previous study of Seyfert 2s (Martini & Pogge 1999). For more than half of our sample, however, corresponding NICMOS images are not available, especially among the Seyfert 1s. Even where NICMOS imaging is available, the small field of view of NICMOS restricts the maps to the central $5''$ – $10''$ or so (Martini & Pogge 1999; Regan & Mulchaey 1999). We therefore need an alternative way to recover this information in the absence of wide-field IR images.

In *V*–*H* color maps such as those we presented in Martini & Pogge (1999), the regions of strong red or blue color that appear are primarily caused by structures that are strongest in the *V*-band images. The *H*-band images, by contrast, are very smooth and appear essentially featureless in all but the most unusual cases. In creating a *V*–*H* color map, we are in effect using the *H*-band image to suppress the underlying starlight distribution in the *V*-band image. The dust and emission structures are certainly visible in the *V*-band images, but their contrast is diminished by the bright stellar background, especially in the innermost regions. The contrast is further reduced in the Seyfert 1s by the strong, unresolved nuclear point source, especially since the core of the PSF is usually completely saturated in these images, and the surrounding $1''$ – $2''$ are contaminated by light from the wings of the WFPC2 PSF (e.g., Biretta et al. 1996).

One way to enhance such fine structural features in single-filter images is to fit the smooth galactic starlight profile with elliptical isophotes and then subtract or divide the

³ IRAF is distributed by the National Optical Astronomy Observatory, which is operated by the Association of Universities for Research in Astronomy, Inc., under a cooperative agreement with the National Science Foundation.

⁴ XVISTA is the direct lineal descendant of Lick Observatory Vista and is maintained in the public domain by a cadre of former Lick graduate students as a service to the community at <http://ganymede.nmsu.edu/holtz/xvista>.

model fit from the images. The fine structure emerges as fit residuals. This is often done to search for dust and other structures in ground-based and *HST* images of elliptical galaxies (e.g., Sparks et al. 1985; McNamara & O’Connell 1993; van Dokkum & Franx 1995; McNamara, O’Connell, & Sarazin 1996; Koekemoer et al. 1999). For the great majority of our galaxies, however, this technique is impractical because the nuclear-region isophotes are generally not elliptical, and isophote fitting fails completely, producing residuals that are more a reflection of the fit’s failure to converge rather than real structures. The presence of a bright saturated nucleus in many of our images makes matters worse.

We have instead devised an alternative approach based on Richardson-Lucy (R-L) image restoration (Richardson 1972; Lucy 1974) applied to *HST* imaging (Snyder, Hammoud, & White 1993) that yields excellent results, as we shall describe and demonstrate. The method is as follows (why it works is described below.) For each cleaned image, we convolve a copy of that image with a model of the PSF for the PC1 camera appropriate to the filter bandpass generated using Tiny Tim (Krist & Hook 1999). We adopted an elliptical galaxy template spectrum for computing the polychromatic model PSF. We then divide the original image by the PSF-smoothed image and further convolve this ratio with the transpose of the model PSF. Mathematically, this procedure produces a final image S defined as

$$S = \left[\frac{I}{I \otimes P} \right] \otimes P^t, \quad (1)$$

where I is the original image, P is the model PSF, P^t is the transpose of the model PSF, $P^t(x, y) = P(-x, -y)$, and \otimes is the convolution operator. (The use of P^t reveals the origins of this technique in R-L restoration, as we describe below). The procedure described above has been implemented as an XVISTA script that performs all of the convolutions in the Fourier domain using fast Fourier transforms.

We call the resulting image S a “structure map” because the process described above has effectively removed most of the larger scale smooth light distribution, highlighting unresolved and marginally resolved structures on the scale of the PSF. Dusty regions appear dark, while compact emission-line regions or clusters (knots) of stars appear bright, much as they would in a color map derived from two images. These maps recover both dust and emission structures with very high fidelity and with fewer artifacts due to mismatched PSFs in the inner regions as seen in visible/IR color maps.

Figures 1–7 and Figure 8 (NGC 1068) show the structure maps for the central 30'' of each of the 43 CfA Seyfert galaxies in our sample. The intensities (*black to white*) show the fractional residuals ($\pm 10\%$) about the original pixel-to-pixel intensity. Dark regions show the locations of dust obscuration, and bright regions are either locations of enhanced stellar light (e.g., star formation regions) or emission-line regions (the F606W filter is wide enough to admit several bright emission lines from high surface brightness regions). Images appear in the same order as listed in Table 1, running from left to right and top to bottom across the figure, in order of Seyfert 1 through Seyfert 2. Within each Seyfert type, the galaxies appear in alphanumeric order by the name listed in column (1) of Table 1. The scale bar in each image panel indicates 1 kpc projected size at the adopted distance

of the galaxy (Table 1, col. [8]). Figure 8 shows NGC 1068 separately, since its close proximity and large physical size allows sampling of particularly fine spatial scales. The left panel of Figure 8 shows an F606W filter image with the same 30'' field of view used in the other structure maps, while the right panel shows the central 10'' of a short-exposure F547M filter image. A detailed description and interpretation of these structure maps is provided in the next section. When referring to images of individual galaxies in the text below, we will give the figure number and the image’s location in the figure the first time it is cited. For example, the image of UM 146 is Figure 5 (*middle right*).

Structure maps of visible-wavelength WFPC2 images are excellent surrogates for color maps, allowing us to recover a great deal of information from a single-band image. To illustrate this, Figure 9 shows (*left*) a $V-H$ color map of the central 5'' of NGC 7674 from Martini & Pogge (1999) and (*right*) the structure map of the same region derived from the V -band image alone using the techniques described above. The structure map shows all of the dust (*dark*) and emission (*bright*) features visible in the $V-H$ color map, but without artifacts due to the mismatch between the WFPC2 and NICMOS PSFs. The structure maps give us two advantages over the $V-H$ color maps derived from WFPC2 and NICMOS images: we can get closer to pointlike nuclei at full WFPC2 resolution (higher than that of NICMOS), and we can recover information across most or all of the $\sim 34''$ PC1 camera field of view, as compared with the $\sim 5''$ field of view of the NIC1 images presented in Martini & Pogge (1999). This greater field of view will be crucial for our analysis, since it will allow us to study any associations between nuclear dust structures and larger scale structures such as bars or disk spiral arms in the host galaxies proper.

Why does it work? The structure map defined above is approximately the “correction image” that emerges from the second iteration of an R-L image reconstruction (see Snyder et al. 1993; Richardson 1972, eqs. [5] and [6]). At the end of each iteration of an R-L reconstruction, the resulting reconstructed image is convolved with the PSF and compared to the original image. A correction image is generated by forming the ratio of the original image to its PSF-convolved reconstruction, which measures the fractional deviation between the model and the original. This information is then used to refine the estimate of the reconstructed image during the next iteration. This correction and comparison process is repeated until the correction image no longer changes significantly, usually because noise and artifacts, relentlessly propagated through each iteration, overwhelm whatever residual structures remain to be reconstructed. After the second iteration, the corrector frame contains the unrecovered structures after the reconstruction has recovered only the first-order, smooth structure in the image (the first iteration in typical implementations compares the original image to a “reconstruction” that contains no structure at all). Our structure map is essentially this second-iteration correction image, which is why it highlights unresolved and marginally resolved high-order structures present in the images. Formally, however, the expression defining the corrector image from the second R-L iteration contains an additional convolution with the transpose of the PSF in the denominator [i.e., $(I \otimes P^t) \otimes P$ instead of $I \otimes P$]. This difference is minor, since operationally it makes the true second-iteration correction frame slightly smoother than our structure map.

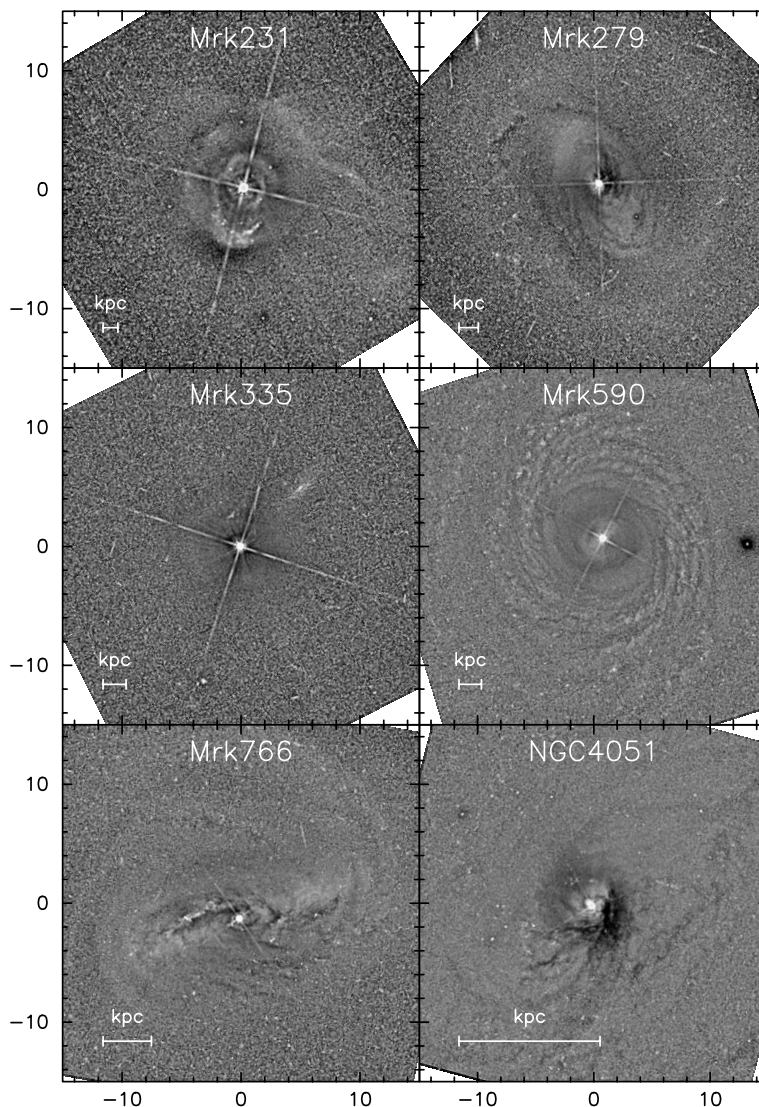


FIG. 1.—Structure maps for Mrk 231, Mrk 279, Mrk 335, Mrk 590, Mrk 766, and NGC 4051. These images show the central $30''$ of each galaxy and intensities (black to white) show the fractional residuals ($\pm 10\%$) about the original pixel-to-pixel intensity. Dark regions show the locations of dust obscuration, and bright regions are either locations of enhanced stellar light (e.g., star formation regions) or emission-line regions. All images have been rotated to orient them with north up and east to the left.

Like any reconstructive technique, structure maps are exquisitely sensitive to noise and artifacts in the images, especially single bright or dead pixels. If these are not removed, the bright negative or positive false stars appear in the structure map images. Other artifacts are the appearance of negative “moats” around very high contrast point sources (either in the nuclei or nearby field stars) and bright spots or smudges near the residuals of cosmic-ray events (we can never completely remove the brightest ion-event trails). Moats are a problem for those images with strongly saturated nuclei. We can eliminate most moats by truncating the nuclear brightness profiles before creating the structure map, allowing us to recover information close to a bright nucleus. In the very brightest nuclei we still lose information despite this. Artifacts due to single bad pixels are removed manually using the interactive pixel zapper (*tvzap*) in XVISTA and then iterating until all of the most obvious artifacts are removed from the subsequent structure maps.

While the structure mapping procedure appears superficially similar to so-called digital unsharp masking (e.g., Heisler & Vader 1994; Walterbos, Braun, & Kennicutt 1994), the results are quite different. To illustrate this, the top two panels of Figure 10 show (*top left*) the central $15''$ of the unprocessed F606W image of NGC 3516 (displayed as logarithmic intensity) and (*top right*) the structure map generated using the method described above. Below these, we show a pair of normalized unsharp-mask images generated using (*bottom left*) a Gaussian kernel with $\text{FWHM} = 2.2$ pixels (the FWHM of the core of the PSF on the PC1 detector in this filter) and (*bottom right*) a 3×3 pixel boxcar kernel (the smallest practical boxcar kernel width). Each of the three maps are displayed to show the same range of dark and bright features. The structure maps created by the method described above are superior in all respects. No choice of Gaussian, boxcar, or other smoothing kernels (e.g., Hanning, cosine bell, etc.) could be found that produced results of comparable quality. In some sense this

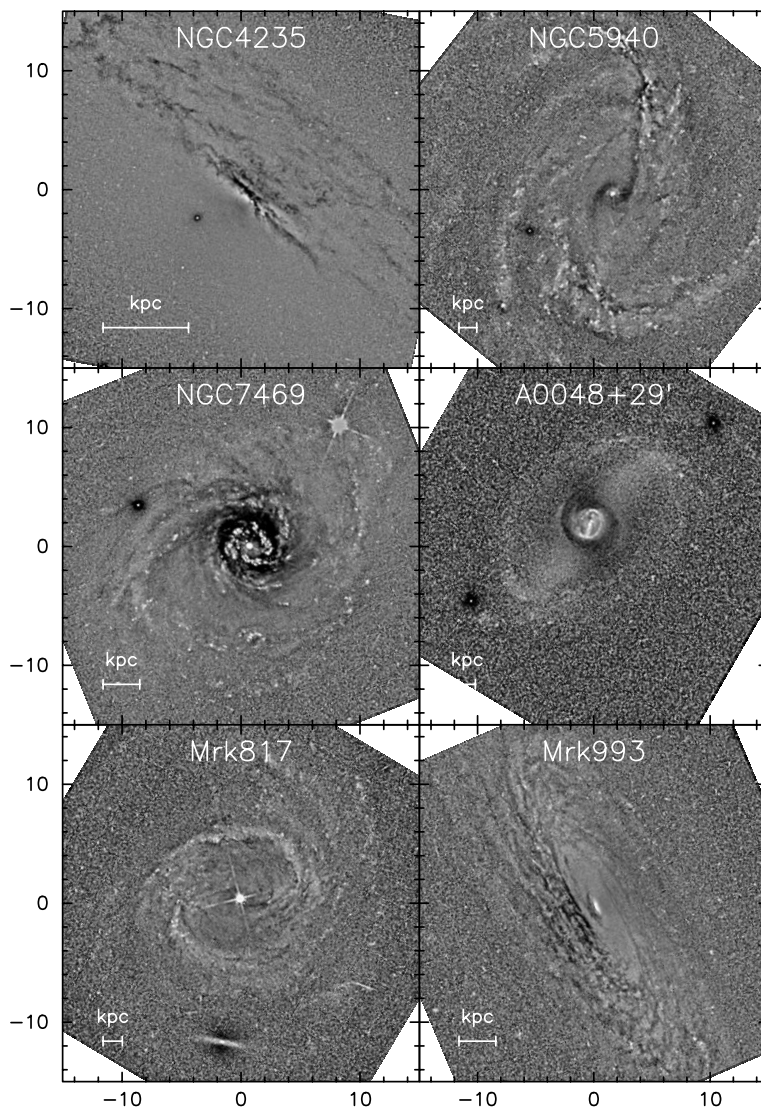


FIG. 2.—Same as Fig. 1, but for NGC 4235, NGC 5940, NGC 7469, A0048+29, Mrk 817, and Mrk 993

should not be surprising, since what passes for unsharp masking in the literature is all too often the result of an arbitrary choice of smoothing kernel. Our method is formally rooted in reconstructive analysis of the images and uses the image PSF, which embodies detailed information about how the original images are formed, including the power in the broad wings surrounding the diffraction-limited core.

5. MORPHOLOGY

5.1. Circumnuclear Structure

The circumnuclear regions of all of the Seyfert galaxies in our sample, with exceptions noted below, have dust and emission regions in the inner kiloparsec. It is immediately evident from the structure maps that the distribution of circumnuclear dust in most of these galaxies takes the form of nuclear dust spirals. By analogy with the spirals arms of galaxy disks, we can characterize them as either “grand design” (clearly delineated and symmetric two-arm spirals) or “flocculent” (spiral form, but broken into many arms). Our structure mapping technique has successfully recovered

all of the spiral dust lanes previously reported in the CfA Seyfert 2s (Martini & Pogge 1999), although we can now trace these structures to larger radii than in the limited field-of-view NICMOS images.

The nuclear dust spirals in most of the galaxies in this sample appear to connect larger scale dust lanes to the S/N limit of the images. Some of these dust lanes form nearly contiguous arms that can be followed for over a full rotation and extend many kiloparsecs in length, such as those in NGC 6104 (Fig. 3, *bottom left*) and Mrk 744 (Fig. 4, *middle left*). The fact that some of these dust lanes extend for kiloparsecs suggest they are relatively long lived and trace the infall of cold dense material from the host galaxy disk. A notable feature of some nuclear spirals is that they are the inner extension of large-scale, often “straight” dust lanes along the edges of large-scale stellar bars in the host galaxies. Particularly striking examples of this are Mrk 766 (Fig. 1, *bottom left*), NGC 5940 (Fig. 2, *top right*), A0048+29 (Fig. 2, *middle right*), Mrk 471 (Fig. 4, *top right*), NGC 5674 (Fig. 5, *middle left*), NGC 5347 (Fig. 7, *top left*), NGC 5695 (Fig. 7, *top right*), and NGC 7674 (Fig. 7, *middle right*). This dust morphology is expected from hydrody-

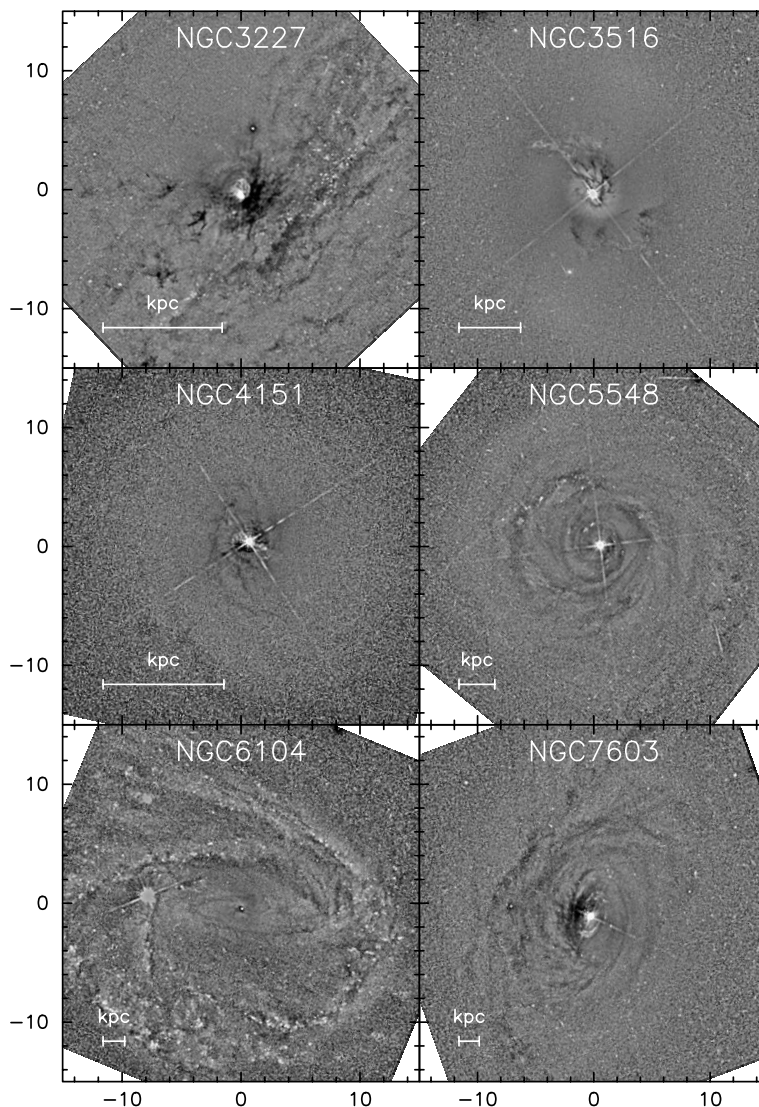


FIG. 3.—Same as Fig. 1, but for NGC 3227, NGC 3516, NGC 4151, NGC 5548, NGC 6104, and NGC 7603

dynamic simulations of the flow of interstellar gas under the influence of large-scale stellar bar potentials (Athanasoula 1992) and is seen in nonactive galaxies, especially in later type barred spirals (e.g., Quillen et al. 1995; Regan, Vogel, & Teuben 1997). We will discuss these structures further in the next section.

While spiral dust lanes are very common, they are not the only dust distribution seen. In some galaxies the distribution of dust is chaotic, having no clear overall pattern. The best examples of this are NGC 3227 (Fig. 3, *top left*), Mrk 266SW (Fig. 6, *bottom left*), and NGC 5929 (Fig. 7, *middle left*). These three galaxies are all strongly interacting, and we will discuss them further below. In two galaxies, NGC 4235 (Fig. 2, *top left*) and NGC 4388 (Fig. 6, *bottom right*), the host galaxy is sufficiently inclined relative to the line of sight that we cannot discern the circumnuclear distribution of the dust. Only a few galaxies show no dust structures on greater than 1 kpc in their nuclei. These are the Seyfert 1s Mrk 231 (Fig. 1, *top left*) and Mrk 335 (Fig. 1, *middle left*) and the dwarf Seyfert 1 NGC 4395 (Fig. 4, *bottom left*), although Mrk 231 does show larger scale structure. The first two are among the most distant objects in our sample and

have extremely prominent nuclei, but there are distant Seyfert 1s that still show structures on small scales despite their distance (e.g., Mrk 279 and Mrk 471). The mottling in the structure map of NGC 4395 is the result of being able to resolve giant stars in this nearby ($D_{75} = 3.6$ Mpc) galaxy. We will not discuss NGC 4395 further. Table 2 gives capsule descriptions of the circumnuclear morphologies revealed by our structure maps.

NGC 5252 (Fig. 5, *top left*) and Mrk 270 (Fig. 5, *bottom right*) have flocculent nuclear spirals embedded in inclined disks on scales of 1–2 kpc. In both cases we see only the half of the disk on the near side of the host galaxy relative to our line of sight; this is the side of the disk that will obscure the most starlight “behind” the disk from our point of view. The far side of the dust disk will be less distinct because there is more galactic starlight between us and the back of the disk. Figure 11 shows the disks outlined in the structure maps.

The flocculent nuclear dust disk in NGC 5252 is the same one found by Tsvetanov et al. (1996) after they divided their WFPC2 continuum images by a smooth elliptical isophote fit. The kinematic properties of this disk, which also appears

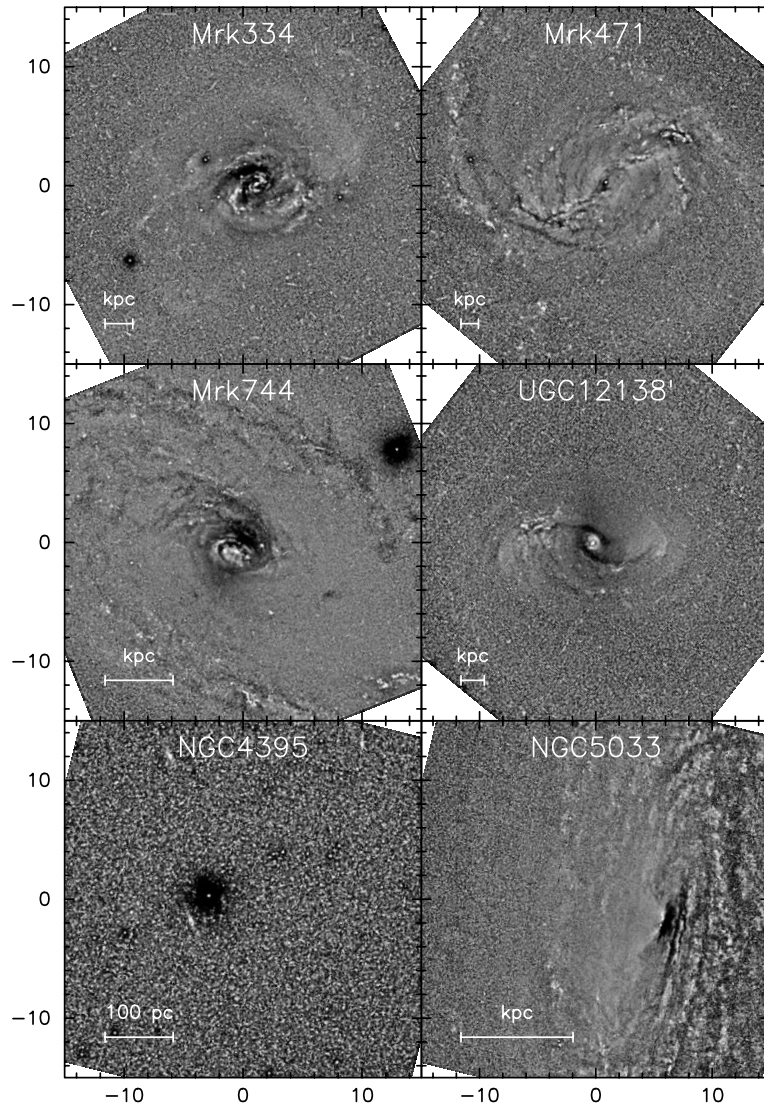


FIG. 4.—Same as Fig. 1, but for Mrk 334, Mrk 471, Mrk 744, UGC 12138, NGC 4395, and NGC 5033

in emission, has been described by Morse et al. (1998). In our structure map images, we find that this disk has an axis ratio of 0.73, implying a disk inclination of $\sim 43^\circ$, with the semimajor axis of $\sim 3''$ (~ 1.3 kpc) oriented along P.A. $\approx 106^\circ$. This orientation is almost exactly perpendicular to the major axis of the host galaxy stellar disk (P.A. $\approx 16^\circ$), but it is misaligned by $\sim 30^\circ$ relative to the axis of the famous ionization cone in this object (P.A. $\approx 163^\circ$; Tadhunter & Tsvetanov 1989). These axes are drawn in Figure 11a for reference.

In Mrk 270, the dusty nuclear disk has a semimajor axis of $\sim 11''$ (~ 2 kpc) oriented along P.A. $\approx 103^\circ$ and is inclined by $\sim 60^\circ$ (axis ratio of ~ 0.5). By comparison, the disk of Mrk 270 is nearly face-on (axis ratio of 0.927 reported by the Two Micron All Sky Survey). Mrk 270 has only small-scale extranuclear emission, seen here as the white filaments between $1''$ and $2''$ northeast of the nucleus in Figure 11b. This emission cannot be characterized as an ionization cone per se (see Pogge 1989b for ground-based [O III] emission-line imaging). It is more likely to be dusty material in the far side of the nuclear disk illuminated and ionized by the nucleus; note how the bright filaments of emission appear

to merge smoothly with the darker (dust) filaments in the foreground.

An additional component of diffuse emission, apparently *stellar* in origin, is seen nearly perpendicular to the gas disks in both of these galaxies. In Mrk 270, this is the diffuse dumbbell-shaped feature aligned along P.A. $\approx 161^\circ$ and extending to a projected radius of $\sim 2''$. This feature is aligned exactly with the major axis of the nuclear stellar bar seen in *H*-band NICMOS images (Martini et al. 2001), and the outer edge of the dumbbell coincides with the ends of the nuclear bar. In NGC 5252, the enhanced starlight is aligned nearly exactly with the major axis of the stellar isophotes along P.A. $= 16^\circ$, but it is less pronounced and lacks the sharp cutoff in radius seen in Mrk 270. Such features are not unusual among the structure maps in our sample. In particular, the ridge lines of the strong stellar bars in Mrk 766, A0048+29, and NGC 5674 (and present but less obvious without contrast enhancement in NGC 5940) appear as excess diffuse light in our structure maps. It is not immediately obvious to us why our structure mapping technique should enhance such features, as they correspond to

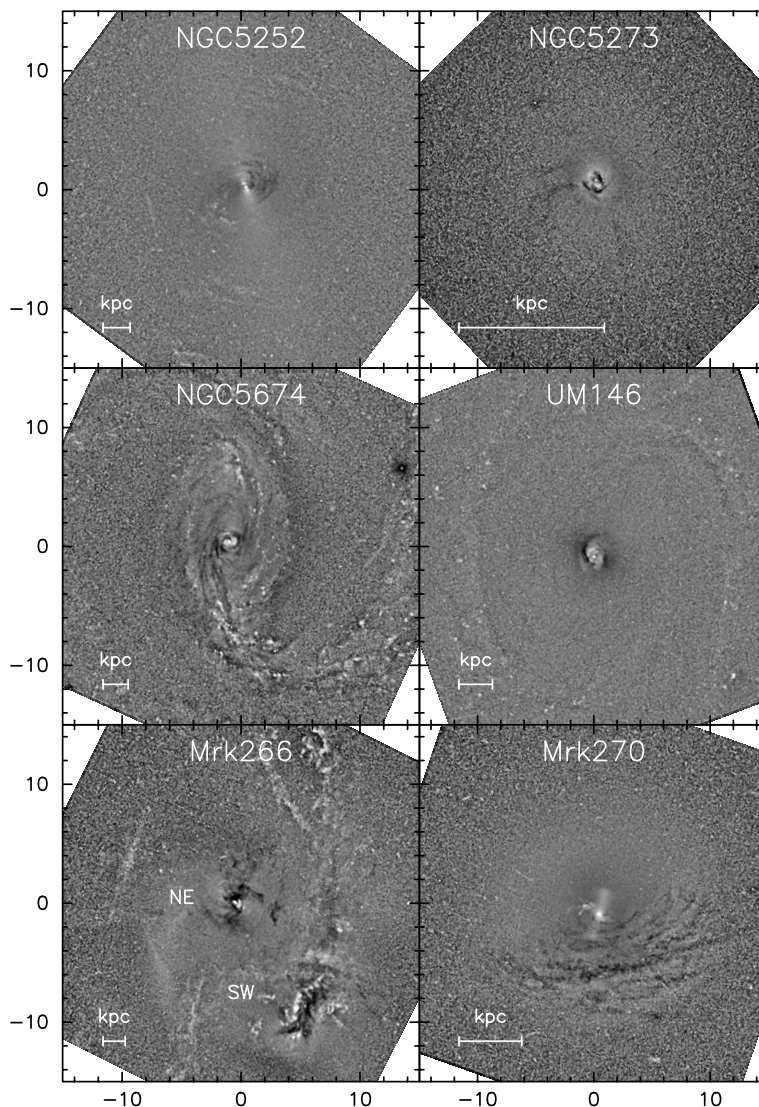


Fig. 5.—Same as Fig. 1, but for NGC 5252, NGC 5273, NGC 5674, UM 146, Mrk 266SW (lower right galaxy in panel), and Mrk 270

structures many times larger than the PSF, but we note that in these latter cases the features we see in the structure map are clearly present in the unenhanced raw images and not artifacts of the enhancement process.

Emission regions appear in the structure maps as bright, often filamentary structures on many scales. The larger scale emission features, such as those seen in Mrk 573 (Fig. 6, *top right*) and NGC 3516 (Fig. 3, *top right*), are previously known from ground-based and space-based imaging (cf. Pogge & DeRobertis 1995 or Ferruit et al. 1999 for Mrk 573; Pogge 1989a for NGC 3516). Some of these regions are on scales of $\lesssim 1''$, such as the small figure-eight (bicone?) of emission we see in NGC 7682 (Fig. 7, *bottom left*) or the S-shaped region interrupted by dust in the nucleus of UGC 6100 (Fig. 7, *bottom right*).

Other “emission” features appearing in the structure maps are bright stellar knots, many appearing along the spiral arms of the host galaxy. Some of these knots of emission can be quite near the nucleus, signaling at least some circumnuclear star formation in these objects. The most obvious example in our sample is the well-known bright starburst ring in NGC 7469 (Fig. 2, *middle left*; Wilson et al.

1991), but not all of these appear to qualify as “starbursts.” Interesting cases, particularly for future study by those interested in circumnuclear star formation, are A0048+29 (a nuclear ring and bar), NGC 7603 (Fig. 3, *bottom right*), Mrk 334 (Fig. 4, *top left*), Mrk 744 (Fig. 4, *middle left*), and NGC 7674 (Fig. 7, *middle right*).

5.2. Large-Scale Bars

About 75% of the host galaxies in the CfA sample are known to be barred (McLeod & Rieke 1995; Knapen et al. 2000). It is in many of these barred galaxies that we find the grand-design nuclear spirals on subkiloparsec scales. Furthermore, most of the spirals are clearly connected to the host galaxy via dust lanes running along the bars. Particular examples are NGC 4235, NGC 5940, Mrk 817, NGC 6104, Mrk 471, UGC 12138, NGC 5674, NGC 5347, NGC 5695, and NGC 7674; all have “straight” dust lanes on large scales in the structure maps in addition to nuclear grand-design spirals. These straight dust lanes are expected for gas and dust compressed in the principal shocks along the leading edges of a bar (e.g., Athanassoula 1992). All but Mrk

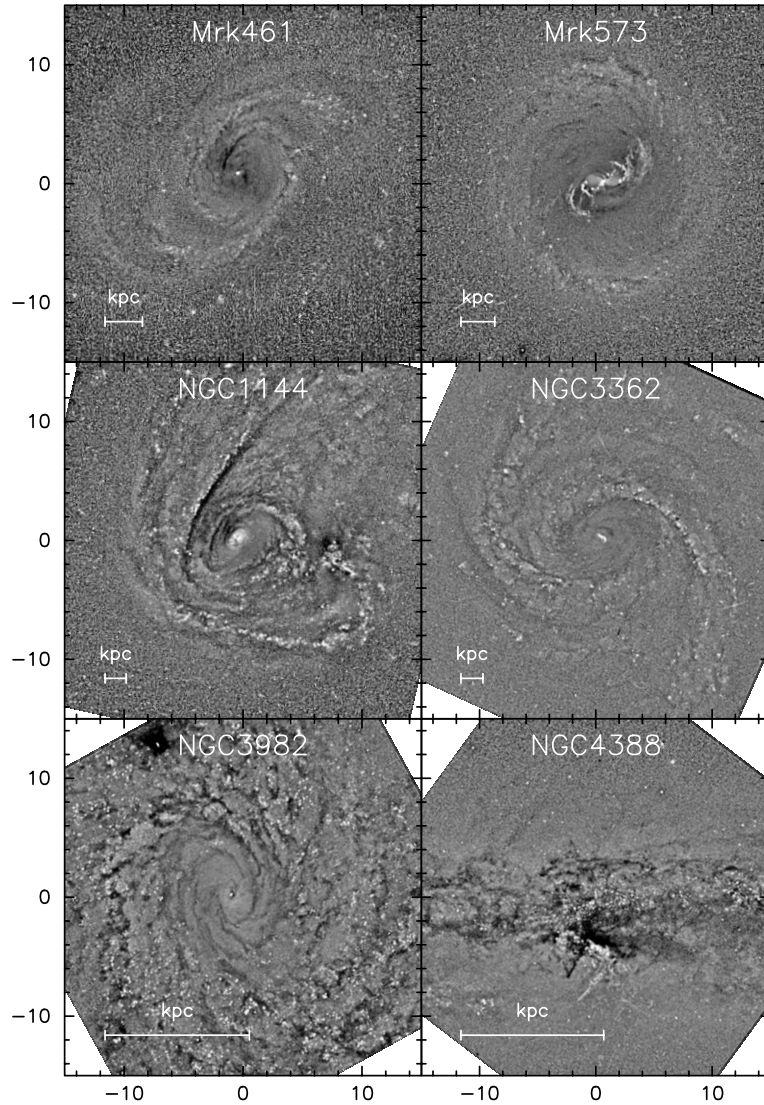


FIG. 6.—Same as Fig. 1, but for Mrk 461, Mrk 573, NGC 1144, NGC 3362, NGC 3982, and NGC 4388

817, NGC 6104, and NGC 5695 have bars strong enough to have led to a barred classification in the RC3 catalog; the RC3 classification for these three galaxies is given as “?”. NGC 6104, NGC 5695, and NGC 7674 were observed to have bars in the *K* band by McLeod & Rieke (1995; noted by the “BIR” in Table 2). They did not observe Mrk 817, although Malkan et al. (1998) report a distinct bar in Mrk 817 in their WFPC2 image (the same image we use to create this structure map), and Knapen et al. (2000) list it as barred in their IR imaging. Mrk 279 shows some evidence for the long, straight dust lanes found in many large-scale bars, but no bar classification is given by either the RC3, McLeod & Rieke (1995), or Malkan et al. (1998), although Knapen et al. (2000) give it a relatively weak bar classification. Only three strongly barred galaxies do not contain circumnuclear grand-design spirals: NGC 7469, NGC 3516, and NGC 5695. NGC 7469 and NGC 5695 may contain them, although the circumnuclear region is difficult to resolve well in these two objects, while NGC 3516 clearly has a multiarm spiral.

Nuclear spiral structure in the gas (and dust) on subkiloparsec scales is predicted by hydrodynamical models of gas

flow in the central regions of barred galaxies. In many cases these spirals were barely resolved by the numerical simulations in the inner kiloparsec due to a decreasing number of SPH particles (e.g., Athanassoula 1992; Englmaier & Gerhard 1997; Patsis & Athanassoula 2000). Recent high-resolution hydrodynamical simulations (Englmaier & Shlosman 2000; Maciejewski et al. 2002), however, show the formation of structures remarkably similar to what we see here in single-barred galaxies on comparable (a few hundred parsecs) scales. The structures are spiral shocks in gas with relatively high sound speeds, leading to gas flows directly into the nucleus (or at least down to the smallest scales resolved by their models). At low sound speeds, they find that the spiral shocks are interrupted by the inner Lindblad resonance and the inflows terminate on a nuclear ring. Only two of our galaxies have nuclear rings: NGC 7469 (Fig. 2, *middle left*) and A0048+29 (Fig. 2, *middle right*).

Interestingly, none of the unbarred galaxies have grand-design nuclear spirals. The nuclear spiral structure in these systems is often multiarm and flocculent in form. The morphology of the nuclear spirals in the Seyfert 2s were pre-

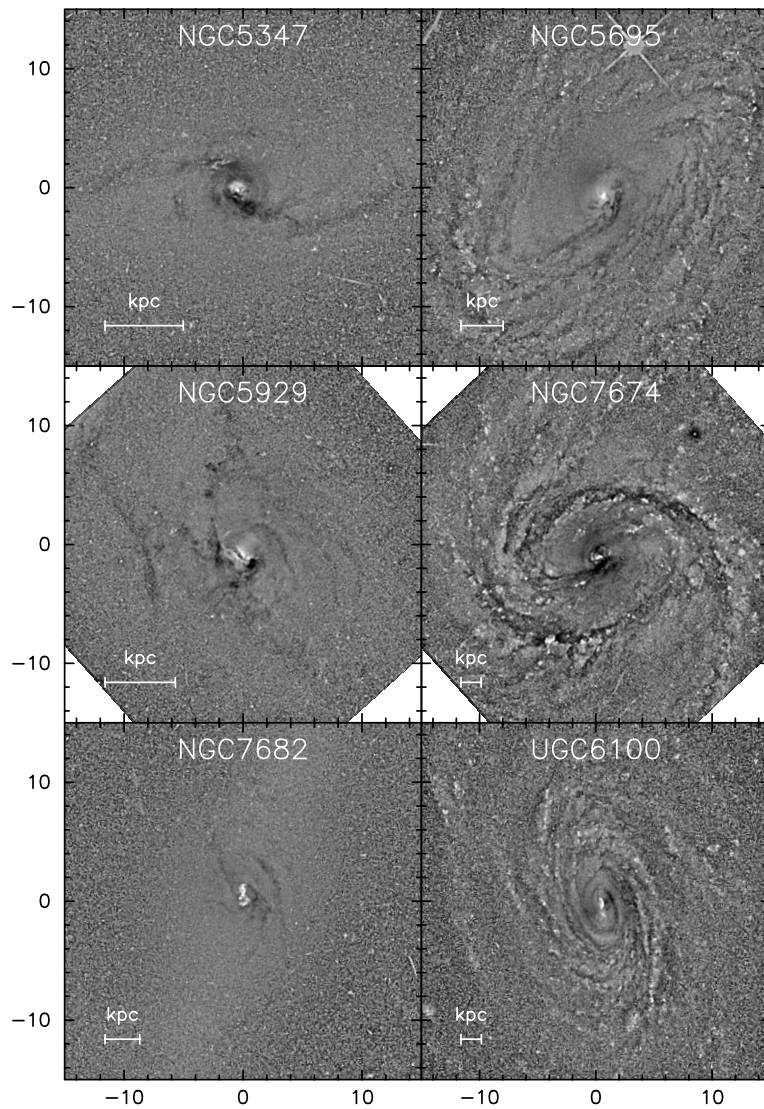


FIG. 7.—Same as Fig. 1, but for NGC 5347, NGC 5695, NGC 5929, NGC 7674, NGC 7682, and NGC 6100

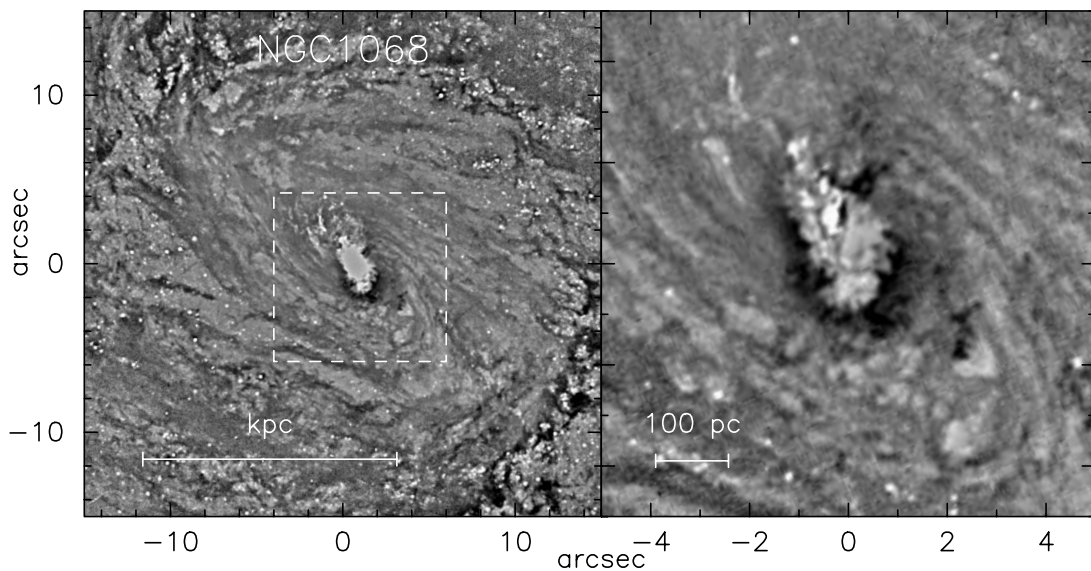


FIG. 8.—*Left*: Same as Fig. 1, but for NGC 1068 and the F606W image. *Right*: Central 10'' of NGC 1068 in the F547M image, corresponding to the dashed box at left.

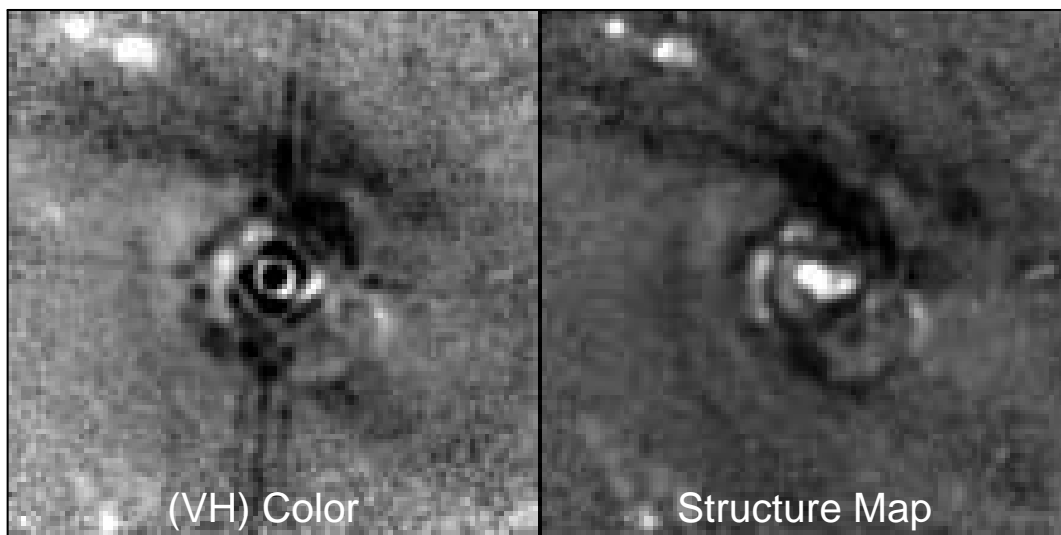


FIG. 9.—Illustration of the ability of structure maps to recover the same dust and emission features seen in $V-H$ color maps for NGC 7674. The $V-H$ color map (left) from Martini & Pogge (1999) clearly shows a two-arm nuclear dust spiral, in addition to a PSF artifact from the bright nuclear source in the H image. The structure map (right) shows the same dust lanes as the color map, although without the NICMOS PSF artifacts. Each panel is $5''$ on a side.

viously described in Martini & Pogge (1999). The Seyfert 1s shown here exhibit similar types of structures. Particularly striking and well-resolved nuclear spirals are apparent in NGC 4051, NGC 3227, NGC 7603, and Mrk 993. NGC 4051 shows some evidence for a grand-design nuclear spiral on roughly kiloparsec scales, but on smaller (several hundred parsecs) scales the structure breaks up into multiarm spirals. The spiral structure in NGC 3227 is very irregular, and the individual components or armlets can rarely be traced for more than 60° . The spirals in NGC 7603 and Mrk 993 are much more regular but appear to have more than two arms. Flocculent spiral structures are found in both barred and unbarred galaxies and could be the result of acoustic or pressure-driven instabilities in the circumnuclear gaseous disks (Elmegreen et al. 1998; Montenegro, Yuan, & Elmegreen 1999).

5.3. Interacting Galaxies

There are three strongly interacting galaxies in this sample: NGC 3227, Mrk 266SW, and NGC 5929. These galaxies have very chaotic dust structures from large scales down to less than a kiloparsec, suggestive of the transport of a significant fraction of the host galaxy's interstellar matter into the central regions. Such massive transport is a feature of hydrodynamical simulations of interacting galaxies (e.g., Barnes & Hernquist 1991, 1992; Mihos & Hernquist 1996; Kennicutt, Schweizer, & Barnes 1998). By contrast, other clearly interacting but decidedly less morphologically disturbed galaxies in our sample, specifically Mrk 744 and NGC 1144, exhibit a relatively ordered and spiral dust morphology down to less than kiloparsec scales. However, both still have very dusty nuclear regions compared to other galaxies in the sample.

Bar modes that might drive gas inflow are expected in minor merger systems, although only after about 1 Gyr has elapsed since the merger between the host and satellite galaxies (Walker, Mihos, & Hernquist 1996). The nearly complete dusty disorder we see in the nuclear regions of the most strongly interacting galaxies suggests that the matter

transport has occurred on less than a dynamical timescale, much faster than the typical slow and steady inflow due to a bar potential. These interacting galaxies clearly have sufficient matter inflow to fuel nuclear activity on the scales probed by these *HST* observations.

6. SEYFERT 1s VERSUS SEYFERT 2s

At first sight, the differences between Seyfert 1s and 2s appears striking, since nearly all of the Seyfert 1s and 1.5s have bright, saturated starlike nuclei showing multiple Airy rings and diffraction spikes, whereas the Seyfert 1.8s, 1.9s, and 2s have fainter, unsaturated nuclei. This strong nuclear brightness contrast was seen by Nelson et al. (1996) in WFPC1 images of Seyfert galaxies and confirmed by Malkan et al. (1998) using a larger WFPC2 imaging survey from which many of our images were derived.

As we shall see, however, the circumnuclear regions do not show such systematic differences between the two types: only the very bright nucleus gives any hint as to the spectral type of the nucleus. A major goal of our study is to determine if there are any differences in the circumnuclear morphologies of these Seyfert 1s and 2s. We inspected each galaxy for evidence of circumnuclear features such as nuclear spirals, bars, and rings, in addition to dust lanes consistent with a large-scale bar feeding gas and dust into this region. Table 2 lists the galaxies from Table 1 and provides their morphological type, angular size (D_{25}), and axis ratio (R_{25}) from the RC3, along with our morphological classifications.

To examine them in detail and take into account the range of distances and sizes of the CfA sample, we first considered a distance-limited subset restricted to galaxies within 100 Mpc in which we can easily resolve structure in the central kiloparsec; more distant galaxies are denoted by a “D” in column (8) of Table 2. In addition, nearly edge-on ($R_{25} > 0.3$) and strongly interacting galaxies were excluded. This leaves us with seven Seyfert 1s and 14 Seyfert 2s. All of these galaxies, with the excep-

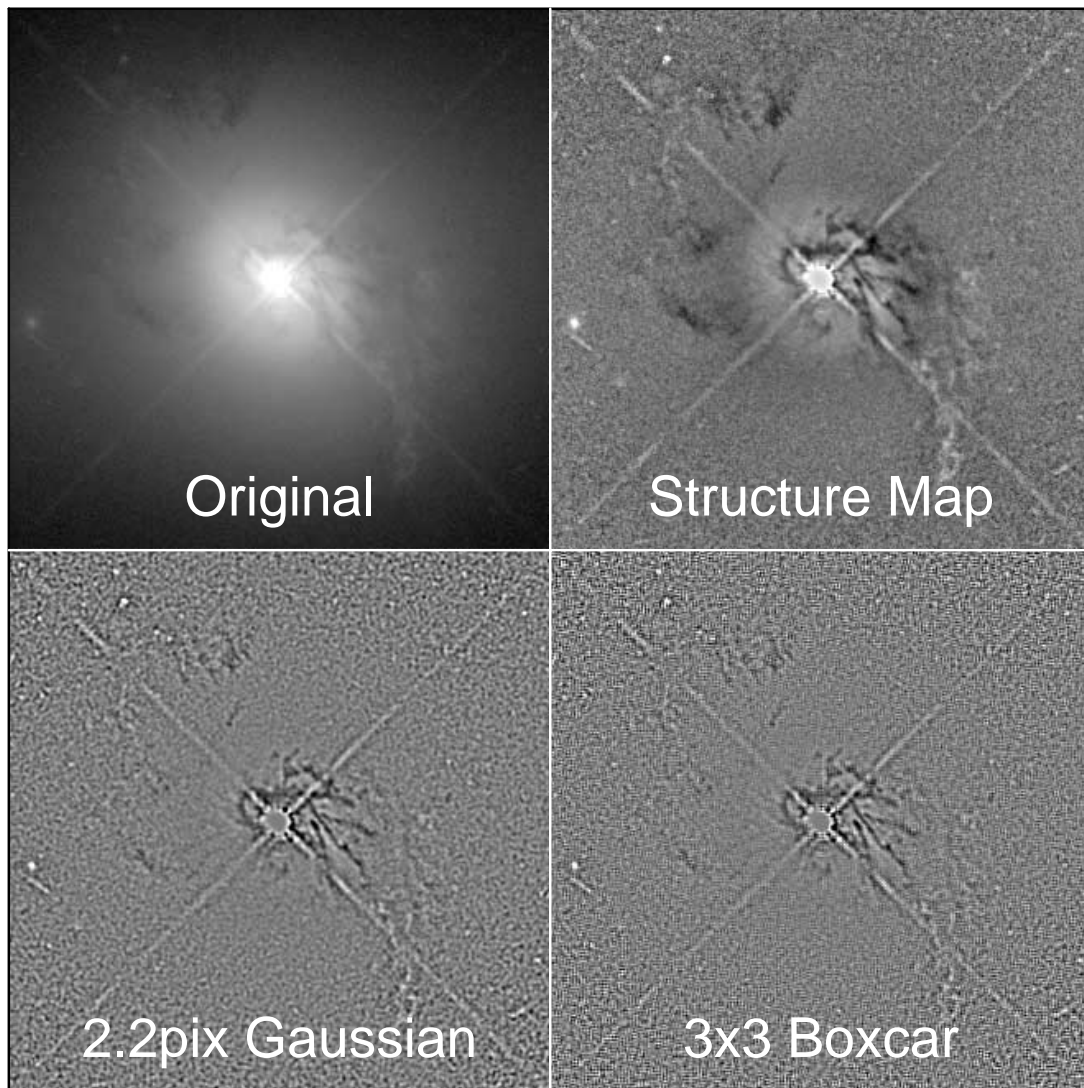


FIG. 10.—Illustration of the difference between structure maps and common unsharp masking techniques for NGC 3516. The original image (*upper left*) shows some evidence of the nuclear dust spirals that are clearly revealed with the structure map (*upper right*). These spirals have much lower contrast when an unsharp masking technique is used, either with a 2.2 pixel wide Gaussian (*lower left*) filter or a 3×3 pixel boxcar (*lower right*) filter. Each panel is $15''$ on a side.

tion of NGC 4395 (which is exceptionally close and small) show evidence for nuclear spiral structure on subkiloparsec scales with no obvious differences in nuclear dust morphology between the Seyfert types. We also formed a size-limited subset in which we took into account the variation in actual physical size of the galaxies. To do this, we computed the projected physical size in kiloparsecs of D_{25} at the distance of the galaxy (col. [6] of Table 2) and then the fraction of this total size contained within the $30''$ cutouts from the PC camera (col. [7] of Table 2). The size-limited subset includes only sufficiently large Seyfert galaxies, defined here as those with less than 50% of the galaxy within the $30''$ images; smaller galaxies are labeled with an “S” in Table 2. This subset contains 9 Seyfert 1s and 16 Seyfert 2s. *All of these galaxies, with the exception again of NGC 4395, also contain nuclear spiral structure independent of Seyfert type.* While the choice of 100 Mpc and 50% for these distance-limited and size-limited subsets is somewhat arbitrary, they do effectively remove the smallest and most distant

galaxies in which we would not be able to clearly resolve circumnuclear structure, regardless of their Seyfert type.

Looking at our entire sample, what we do not see is a tendency for Seyfert 2 nuclei to be more frequently crossed by host galaxy dust lanes, as found by Malkan et al. (1998) for a larger but arguably more heterogeneous sample of Seyfert galaxies. This is likely the result of the different Hubble type distributions of our respective samples. The median Seyfert 1 host studied by Malkan et al. (1998) is earlier than the median Seyfert 2 type, while the Seyfert 1s and 2s we study have a similar Hubble type distribution. This difference in host galaxy type can explain why Malkan et al. (1998) found that Seyfert 2s were dustier than Seyfert 1s, whereas we do not find a similar trend. Within the context of the standard unification hypothesis, Malkan et al. (1998) invoke the apparent differences in the circumnuclear environments of Seyfert 1s and 2s to posit that galactic dust on hundreds of parsec scales could obscure Seyfert 1s and make them appear as Seyfert 2s. They suggest that this “galactic dust model” is a viable alternative to the classical torus model

TABLE 2
MORPHOLOGICAL PROPERTIES

Galaxy	Type	RC3 ^a	D_{25} ^a	R_{25} ^a	D_{25} ^b (kpc)	30'' Fraction ^c	Notes ^d
Mrk 231	1	.SAT5\$P	1.12 (0.06)	0.13 (0.05)	63.4	0.38	D, NS, Z
Mrk 279	1	.L.....	0.94 (0.06)	0.23 (0.03)	31.4	0.57	D, S, NS, B?
Mrk 335	1	.	0.5 (0.14)	0 (0.12)	9.8	1.58	D, S, Z
Mrk 590	1	.SAS1*	1.03 (0.03)	0.03 (0.04)	33.3	0.47	D, NB
Mrk 766	1	PSBS1*	0.98 (0.04)	0.06 (0.04)	14.1	0.52	S, NS(GD), B, BIR
NGC 4051	1	.SXT4..	1.72 (0.02)	0.13 (0.02)	26.0	0.10	NS
NGC 4235	1	.SAS1./	1.62 (0.02)	0.65 (0.02)	34.8	0.12	INC
NGC 5940	1	.SB.2..	0.9 (0.07)	0 (0.05)	31.2	0.63	D, S, NS(GD), B, BIR
NGC 7469	1	PSXT1..	1.17 (0.02)	0.14 (0.03)	28.8	0.34	NS, NR, BIR
A0048 + 29	1	PSBS3..	0.95 (0.07)	0 (0.05)	38.1	0.56	D, S, NS, NR, NB, BIR
Mrk 817	1.5	.S?....	0.81 (0.11)	0 (0.06)	24.0	0.77	D, S, NS(GD), B
Mrk 993	1.5	.S..1..	1.34 (0.02)	0.52 (0.03)	41.4	0.23	INC, NS
NGC 3227	1.5	.SXS1P.	1.73 (0.02)	0.17 (0.03)	32.2	0.09	NS
NGC 3516	1.5	RLBS0*	1.24 (0.03)	0.11 (0.04)	19.7	0.29	NS, BIR
NGC 4151	1.5	PSXT2*	1.8 (0.02)	0.15 (0.03)	37.3	0.08	NS
NGC 5548	1.5	PSAS0..	1.16 (0.02)	0.05 (0.03)	28.2	0.35	NS
NGC 6104	1.5	.S?....	0.92 (0.07)	0.08 (0.05)	27.5	0.60	D, S, NS(GD), B, BIR
NGC 7603	1.5	.SAT3*P	1.19 (0.04)	0.18 (0.04)	53.3	0.32	D, NS
Mrk 334	1.8	.P.....	0.99 (0.05)	0.14 (0.04)	25.1	0.51	S, NS
Mrk 471	1.8	.SB.1..	0.95 (0.05)	0.19 (0.04)	35.6	0.56	D, S, NS(GD), B
Mrk 744	1.8	.SXT1P.	1.34 (0.02)	0.23 (0.03)	23.0	0.24	NS
UGC 12138	1.8	.SB.1..	0.92 (0.07)	0.08 (0.05)	24.9	0.60	D, S, NS(GD), B, BIR
NGC 4395	1.9	.SAS9*	2.12 (0.01)	0.08 (0.02)	13.8	0.04	Z
NGC 5033	1.9	.SAS5..	2.03 (0.01)	0.33 (0.02)	58.3	0.05	INC, NS
NGC 5252	1.9	.L.....	1.14 (0.09)	0.21 (0.05)	36.4	0.36	NS
NGC 5273	1.9	.LAS0..	1.44 (0.03)	0.04 (0.04)	13.2	0.18	NS
NGC 5674	1.9	.SX.5..	1.04 (0.06)	0.02 (0.05)	31.3	0.46	NS(GD), B, BIR
UM 146	1.9	.SAT3..	1.1 (0.04)	0.1 (0.04)	26.2	0.40	NS, BIR
Mrk 266SW	2	.P.....	1.08 (0.06)	0.05 (0.05)	38.8	0.42	D, INT
Mrk 270	2	.L...?	1.03 (0.08)	0.04 (0.03)	11.9	0.47	NS, NB
Mrk 461	2	.S.....	0.87 (0.05)	0.13 (0.05)	15.1	0.67	NS
Mrk 573	2	RLXT + *	1.13 (0.07)	0.01 (0.04)	27.9	0.37	NS(GD), NB, BIR
NGC 1068	2	RSAT3..	1.85 (0.01)	0.07 (0.02)	29.7	0.07	NS
NGC 1144	2	.RING. B	1.04 (0.08)	0.21 (0.06)	37.1	0.46	D, NS
NGC 3362	2	.SX.5..	1.15 (0.05)	0.11 (0.05)	44.7	0.35	D, NS
NGC 3982	2	.SXR3*	1.37 (0.02)	0.06 (0.03)	11.6	0.21	NS
NGC 4388	2	.SAS3*/	1.75 (0.01)	0.64 (0.02)	27.5	0.09	INC
NGC 5347	2	PSBT2..	1.23 (0.04)	0.1 (0.04)	18.1	0.29	NS(GD), B, BIR
NGC 5695	2	.S?....	1.19 (0.05)	0.15 (0.05)	25.6	0.32	NS, B, BIR
NGC 5929	2	.S..2*P	0.98 (0.06)	0.03 (0.04)	10.7	0.52	S, INT, NS
NGC 7674	2	.SAR4P.	1.05 (0.03)	0.04 (0.04)	38.7	0.45	D, NS(GD), B, BIR
NGC 7682	2	.SBR2..	1.09 (0.04)	0.05 (0.04)	25.3	0.41	NS, BIR
UGC 6100	2	.S..1?.	0.92 (0.07)	0.18 (0.05)	28.5	0.60	D, S, NS

^a Data taken from the RC3 catalog.

^b Projected size of D_{25} in kiloparsecs at the distance of the galaxy.

^c Fraction of D_{25} contained within our 30'' structure maps.

^d Codes for the morphological classifications. D: distance greater than 100 Mpc (assuming $H_0 = 75 \text{ km s}^{-1} \text{ Mpc}^{-1}$); INC: high inclination ($R_{25} > 0.3$); INT: strongly interacting system; Z: no resolved structure in central kiloparsec; NR: nuclear ring; NS: nuclear spiral; NS(GD): grand-design nuclear spiral; B: straight dust lanes indicative of a large-scale bar in the structure map; BIR: bar found in the K -band by McLeod & Rieke 1995.

(Antonucci 1993), in which the obscuration that gives rise to the Seyfert 1/2 dichotomy lies on parsec scales.

We do, however, have examples of nuclei obscured by host-galaxy dust in our sample; particularly striking examples are the interacting galaxies Mrk 266SW (Fig. 5, *bottom left*) and NGC 5929 (Fig. 7, *middle left*) and the edge-on galaxy NGC 4388 (Fig. 6, *bottom right*), where the nuclei are only visible at IR wavelengths (e.g., Martini et al. 2001). These examples offer qualitative support of the galactic dust model. The fact that we find similar circumnuclear structure in Seyfert 1s and 2s at fixed Hubble type does not refute the

galactic dust model, since the actual dust structures responsible for the nuclear obscuration in any given Seyfert 2 are still likely to be unresolved in most cases (with perhaps the few exceptions noted above) due to the small sizes of molecular clouds. We suspect that the root cause of our discrepancy with the results of Malkan et al. (1998) reflects differences in the distribution of host galaxy morphological types between the Seyfert 1s and 2s in the respective samples. The different distributions in the Malkan et al. (1998) sample may result from the fact that most of the galaxies in their sample are Markarian Seyfert galaxies selected on the

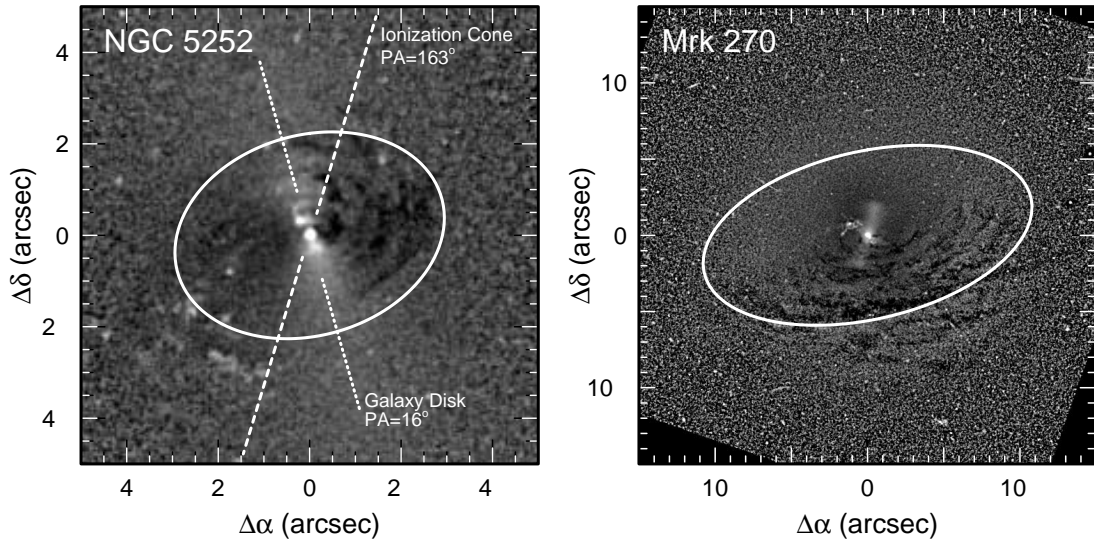


FIG. 11.—Dusty nuclear disks in (left) NGC 5252 and (right) Mrk 270. The scale is indicated in arcseconds. Each panel shows the structure map for the galaxy, with an ellipse illustrating the measured major axis, ellipticity, and position angle of the dust disk. In NGC 5252, we draw the axes of the galaxy disk and the ionization cone for reference. Mrk 270 is nearly face-on and has no ionization cone, but there is filamentary emission-line gas that appears to be illuminated material in the far side of the nuclear disk.

basis of UV excess. By contrast, samples such as the CfA Seyfert galaxies presented here and the Palomar Seyfert galaxies (Ho, Filippenko, & Sargent 1997) have similar Hubble type distributions between Seyfert 1s and 2s, and these surveys are both based on spectroscopy of large numbers of galaxies in a flux-limited survey.

7. CONCLUSIONS

Using a new “structure mapping” technique, we have found nuclear spiral dust structures that are plausibly related to the inflow of interstellar gas from the host galaxies into the nuclear regions of a well-defined sample of Seyfert galaxies. We find the dust morphology that is expected if interstellar gas is being driven primarily by large-scale bars and if interstellar gas is mass-transported inward by torques arising from tidal interactions. There is also circumstantial evidence for the spiral infall of gas, with greater or lesser degrees of coherence, in galaxies that show neither stellar bars nor evidence of tidal interaction. In most cases the spiral dust structures seen previously at small scales in more traditional color maps are shown to be connected to the large-scale properties of the galaxies, although they are not simply continuations of the large-scale features. All of these structures are consistent with the idea that interstellar gas from the host galaxy may be transported into the nucleus, to varying degrees of intensity and coherence, via a variety of mechanisms.

The case that these structures are related to fueling the AGNs is primarily phenomenological. Theoretical models of gas inflow in barred and interacting galaxies predict structures similar in appearance to those we see in our images. What we do not know, however, is whether we can make the final connection between these larger scale structures and the central black hole. That we find these structures in most of the Seyfert galaxies studied here makes this connection plausible, but we cannot yet make it conclusively. From an observational perspective, a particularly difficult challenge is how to establish kinematic evidence of

inflow in cold interstellar material on these scales. From the theoretical side, work on what inflow rates are expected and what observational factors (either in addition to or in the absence of direct kinematical measurements) might help inform such estimations on an object-by-object basis.

It has long been known that bars and interactions occur in inactive galaxies, and there is no reason to expect that they will not funnel gas into the inner regions of those galaxies in much the same way. Further, nuclear spirals have been observed in a number of normal spiral galaxies without obvious AGN activity (Phillips et al. 1996; Carollo, Stiavelli, & Mack 1998; Elmegreen et al. 1998; Laine et al. 1999). If nuclear spirals are signatures of shocks that can dissipate sufficient angular momentum to fuel a black hole, the question remains why normal galaxies that exhibit such structures are not active, particularly as it is now clear that essentially all galaxies harbor nuclear black holes, with masses closely correlated with their host galaxy properties (e.g., Richstone et al. 1998). This suggests that the transport of gas into the central (less than 100 pc) region is a necessary but not unique requirement of nuclear activity.

The near ubiquity of coherent, circumnuclear dust structures suggestive of shocks and matter inflow supports the conjecture that they are responsible for fueling their AGNs. The first step to test this is a study of a well-defined control sample of quiescent spiral galaxies of similar morphological type observed and analyzed in similar ways to the Seyfert galaxies. We are currently engaged in an ongoing *HST* snapshot program to address this question of the relative frequency and strength of nuclear dust spirals in normal galaxies compared to AGNs. More data will be forthcoming.

We wish to thank P. Osmer, B. Peterson, A. Gould, D. Weinberg, S. Mathur, L. Ho, M. Regan, J. Mulchaey, D. Maoz, and M. Malkan for valuable discussions and suggestions. The anonymous referee is also thanked for help improving the final paper. This research has made extensive use of a number of electronic databases, including the

NASA Astrophysics Data System Abstract Service, the NASA/IPAC Extragalactic Database (NED), and the NASA/IPAC Infrared Science Archive. These latter two are operated by the Jet Propulsion Laboratory, California Institute of Technology, under contract with NASA. Primary support for this work was provided by NASA

grant AR-06380.01-A, with additional support from the NICMOS imaging program supported by GO-07867.01-A, both grants from the Space Telescope Science Institute, which is operated by the Association of Universities for Research in Astronomy, Inc., under NASA contract NAS 5-26555.

REFERENCES

- Adams, T. F. 1977, *ApJS*, 33, 19
- Alonso-Herrero, A., Ward, M. J., & Kotilainen, J. K. 1996, *MNRAS*, 278, 902
- Antonucci, R. R. J. 1993, *ARA&A*, 31, 473
- Athanassoula, E. 1992, *MNRAS*, 259, 345
- Barnes, J. E., & Hernquist, L. E. 1991, *ApJ*, 370, L65
- . 1992, *ARA&A*, 30, 705
- Bertin, G., Lin, C. C., Lowe, S. A., & Thurstans, R. P. 1989, *ApJ*, 338, 78
- Biretta, J. A., et al. 1996, *WFPC2 Instrument Handbook*, Ver. 4.0 (Baltimore: STScI)
- Carollo, C. M., Stiavelli, M., & Mack, J. 1998, *AJ*, 116, 68
- Dahari, O., & DeRobertis, M. M. 1988, *ApJS*, 67, 249
- DeRobertis, M. M., Hayhoe, K., & Yee, H. K. C. 1998, *ApJ*, 496, 93
- Elmegreen, B. G., Elmegreen, D. M., & Montenegro, L. 1992, *ApJS*, 79, 37
- Elmegreen, B. G., et al. 1998, *ApJ*, 503, L119
- Englmaier, P., & Gerhard, O. 1997, *MNRAS*, 287, 57
- Englmaier, P., & Shlosman, I. 2000, *ApJ*, 528, 677
- Ferruit, P., et al. 1999, *ApJ*, 523, 147
- Friedli, D., & Benz, W. 1993, *A&A*, 268, 65
- Fuentes-Williams, T., & Stocke, J. T. 1988, *AJ*, 96, 1235
- Heisler, C. A., & Vader, J. P. 1994, *AJ*, 107, 35
- Hernquist, L. E. 1989, *Nature*, 240, 687
- Hernquist, L., & Mihos, J. C. 1995, *ApJ*, 448, 41
- Ho, L. C., Filippenko, A. V., & Sargent, W. L. W. 1997, *ApJS*, 112, 315
- Ho, L. C., & Ulvestad, J. S. 2001, *ApJS*, 133, 77
- Huchra, J., & Burg, R. 1992, *ApJ*, 393, 90
- Huchra, J., Davis, M., Latham, D., & Tonry, J. 1983, *ApJS*, 52, 89
- Keel, W. C. 1996, *AJ*, 111, 696
- Keel, W. C., Kennicutt, R. C., Jr., van der Hulst, J. K., & Hummel, E. 1985, *AJ*, 90, 708
- Kennicutt, R. C., Schweizer, F., & Barnes, J. E. 1998, in *Galaxies: Interactions and Induced Star Formation*, Saas-Fee Advanced Course 26, ed. D. Friedli, L. Martinet, & D. Pfenniger (Berlin: Springer)
- Knapen, J. H., Shlosman, I., & Peletier, R. F. 2000, *ApJ*, 529, 93
- Koekemoer, A. M., O'Dea, C. P., Sarazin, C. L., McNamara, B. R., Donahue, M., Voit, G. M., Baum, S. A., & Gallimore, J. F. 1999, *ApJ*, 525, 621
- Kotilainen, J. K., Ward, M. J., Boisson, C., DePoy, D. L., Smith, M. G., & Bryant, L. R. 1992, *MNRAS*, 256, 125
- Krist, J., & Hook, R. 1999, *The Tiny Tim User's Guide*, Ver. 5.0 (Baltimore: STScI)
- Laine, S., Knapen, J. H., Pérez-Ramírez, D., Doyon, R., & Nadeau, D. 1999, *MNRAS*, 302, L33
- Laine, S., Shlosman, I., Knapen, J. H., & Peletier, R. F. 2002, *ApJ*, 567, 97
- Lucy, L. B. 1974, *AJ*, 79, 745
- Maciejewski, W., Teuben, P. J., Sparke, L. S., & Stone, J. M. 2002, *MNRAS*, 329, 502
- Malkan, M. A., Gorjian, V., & Tam, R. 1998, *ApJS*, 117, 25
- Martini, P., & Pogge, R. W. 1999, *AJ*, 118, 2646
- Martini, P., Pogge, R. W., Ravindranath, S., & An, J. H. 2001, *ApJ*, 562, 139
- McLeod, K. K., & Rieke, G. H. 1995, *ApJ*, 441, 96
- McNamara, B. R., & O'Connell, R. W. 1993, *AJ*, 105, 417
- McNamara, B. R., O'Connell, R. W., & Sarazin, C. L. 1996, *AJ*, 112, 91
- Mihos, J. C., & Hernquist, L. 1996, *ApJ*, 464, 641
- Montenegro, L. E., Yuan, C., & Elmegreen, B. G. 1999, *ApJ*, 520, 592
- Morse, J. A., Cecil, G., Wilson, A. S., & Tsvetanov, Z. I. 1998, *ApJ*, 505, 159
- Mulchaey, J. S., & Regan, M. W. 1997, *ApJ*, 482, L135
- Nelson, C. H., MacKenty, J. W., Simkin, S. M., & Griffiths, R. E. 1996, *ApJ*, 466, 713
- Osterbrock, D. E. 1981, *ApJ*, 249, 462
- Osterbrock, D. E., & Martel, A. 1993, *ApJ*, 414, 552
- Patsis, P. A., & Athanassoula, E. 2000, *A&A*, 358, 45
- Petrosian, A. R. 1982, *Astrophysics*, 18, 312
- Pfenniger, D., & Norman, C. 1990, *ApJ*, 363, 391
- Phillips, A. C., Illingworth, G. D., MacKenty, J. W., & Franx, M. 1996, *AJ*, 111, 1566
- Piner, B. G., Stone, J. M., & Teuben, P. J. 1995, *ApJ*, 449, 508
- Pogge, R. W. 1989a, *AJ*, 98, 124
- . 1989b, *ApJ*, 345, 730
- . 1997, in *ASP Conf. Ser. 113, Emission Lines in Active Galactic Nuclei: New Methods and Techniques*, ed. B. M. Peterson, F.-Z. Cheng, & A. S. Wilson (San Francisco: ASP), 378
- Pogge, R. W., & DeRobertis, M. M. 1995, *ApJ*, 451, 585
- Quillen, A. C., Alonso-Herrero, A., Rieke, M. J., McDonald, C., Falcke, H., & Rieke, G. H. 1999, *ApJ*, 525, 685
- Quillen, A. C., Frogel, J. A., Kenney, J. P. D., Pogge, R. W., & DePoy, D. L. 1995, *ApJ*, 441, 549
- Regan, M. W., & Mulchaey, J. S. 1999, *AJ*, 117, 2676
- Regan, M. W., Vogel, S. N., & Teuben, P. J. 1997, *ApJ*, 482, L143
- Richardson, W. H. 1972, *J. Opt. Soc. Am.*, 62, 55
- Richstone, D., et al. 1998, *Nature*, 395 (Suppl.), A14
- Schmidt, M. 1968, *ApJ*, 151, 393
- Schmitt, H. R. 2001, *AJ*, 122, 2243
- Schwartz, M. 1981, *ApJ*, 247, 77
- Shlosman, I., Frank, J., & Begelman, M. C. 1989, *Nature*, 338, 45
- Snyder, D. L., Hammoud, A. M., & White, R. L. 1993, *J. Opt. Soc. Am. A*, 10, 1014
- Sparks, W. B., Wall, J. V., Thorne, D. J., Jordan, P. R., van Breda, I. G., Rudd, P. J., & Jorgensen, H. E. 1985, *MNRAS*, 217, 87
- Tadhunter, C., & Tsvetanov, Z. 1989, *Nature*, 341, 422
- Toomre, A., & Toomre, J. 1972, *ApJ*, 178, 623
- Tsvetanov, A. I., Morse, J. A., Wilson, A. S., & Cecil, G. 1996, *ApJ*, 458, 172
- van Dokkum, P. G., & Franx, M. 1995, *AJ*, 110, 2027
- Walker, I. R., Mihos, C. J., & Hernquist, L. 1996, *ApJ*, 460, 121
- Walterbos, R. A. M., Braun, R., & Kennicutt, R. C. 1994, *AJ*, 107, 184
- Wilson, A. S., Helfer, T. T., Haniff, C. A., Ward, M. J. 1991, *ApJ*, 381, 79
- Yahil, A., Tammann, G. A., & Sandage, A. 1977, *ApJ*, 217, 903